communications biology

A Nature Portfolio journal

Article

https://doi.org/10.1038/s42003-025-07880-9

HIF1A facilitates hypoxia-induced changes in H3K27ac modification to promote myometrial contractility

Kaiyuan Ji[1,2], Bolun Wen[1,2], Xiaodi Wang[1], Lina Chen[1], Yunshan Chen[1], Lele Wang[1], Junjie Bao[1], Xiuyu Pan[1], Guozheng Zhang[1], Yanmin Jiang[1] ✉ & Huishu Liu[1] ✉

Prior studies have established that myometrial hypoxia during labor is pivotal in intensifying contractions, the alterations in gene expression and histone modifications in myometrial cells under hypoxia have yet to be documented. Here, hypoxia's enhancement of cellular contractility was confirmed, and RNA-seq identified 2,262 differentially expressed genes in human myometrial smooth muscle cells (hMSMCs) under hypoxia. Chromatin immunoprecipitation (ChIP), high-throughput chromosome conformation capture followed by ChIP (Hi-ChIP) were employed to investigate the epigenetic changes, specifically histone modifications (H3K27ac, H3K4me1, H3K27me3, and H3K4me3), in hMSMCs under hypoxia. We identified the enhancer and super-enhancer regions in hMSMCs and found HIF1A as the key mediator of these H3K27ac changes under hypoxia. Labor-associated genes regulated by HIF1A have been identified. Validation experiments on these genes such as *CXCL8, RUNX1*, *IL-6*, and *PTGES3* demonstrated that HIF1A knockdown reduces their expression and associated H3K27ac modifications in peak regions of their promoters or enhancers. These findings indicate that HIF1A probably mediate changes in histone H3K27ac modifications to regulate myometrial cell contractions under hypoxia, providing potential therapeutic and intervention targets for disorders related to parturition.

Moderate uterine contractions are essential for successful labor. Insufficient contractions can cause prolonged labor, obstructed fetal descent, while overly strong contractions can reduce fetal oxygen supply, leading to fetal distress and neonatal asphyxia[1–3]. Despite extensive research, the mechanisms regulating uterine contractions are not fully understood. A significant research gap exists in understanding the molecular mechanisms of uterine contractions and methods to regulate myometrial contractility[4]. Detailed studies of these mechanisms are crucial for identifying molecular targets for abnormal labor progression, postpartum hemorrhage, thus enhancing both fundamental research and precise clinical treatment.

Human myometrial smooth muscle cells (hMSMCs) are central to generating uterine contractions during labor[5]. Multi-omics studies have revealed significant changes in myometrial gene expression during labor, with differentially expressed genes (DEGs) enriched in hypoxia-related pathways[5–7]. Intermittent contractions during labor compress muscle blood vessels, reducing blood flow and creating a transient hypoxic environment in the myometrium[8,9]. Evidence from tissue and cellular experiments underscores the pivotal role of hypoxia in continually enhancing uterine contractions, even with oxytocin administration or oxytocin receptor inhibition, highlighting its significance in strengthening these contractions[10,11]. This strengthening effect can last up to 12 h[8]. Hypoxia-inducible factor 1 A (HIF1A) is the primary transcription factor responsible for cellular responses to hypoxia[10,12,13]. Under hypoxic conditions, reduced activity of prolyl hydroxylases (PHDs) decreases HIF1A hydroxylation, leading HIF1A escapes recognition and ubiquitination by the Von Hippel-Lindau (VHL) complex, then avoiding proteasomal degradation, accumulating in the nucleus, and activating downstream gene expression[14,15]. HIF1A expression has been shown to increase in the myometrium during labor[16,17], and knockdown of HIF1A significantly reduces myometrial contractility in vitro[11,18]. Our previous research demonstrated that HIF1A upregulated genes include *GJA1* and *OXTR*, which promote contractions[18]. HIF1A promotes a metabolic shift from aerobic respiration to anaerobic glycolysis, enhancing cellular adaptability to hypoxia and providing a protective mechanism for tissues, such as tumor or myocardium[19]. We found that

[1]Guangzhou Key Laboratory of Maternal-Fetal Medicine, Institute of Reproductive Health and Perinatology, Guangzhou Women and Children's Medical Center, Guangzhou Medical University, Guangzhou, Guangdong, China. [2]These authors contributed equally: Kaiyuan Ji, Bolun Wen.
✉e-mail: 13189081153@163.com; huishuliu@hotmail.com

HIF1A promotes *SERPINE1*/*ATP5PF* axis, which supports oxidative phosphorylation after hypoxic stress in hMSMCs[11,18]. These findings represent only part of the HIF1A-regulated gene network, necessitating further research to fully elucidate the molecular mechanisms involved. Moreover, the mechanisms by which HIF1A regulates gene expression in hMSMCs need to be explored and validated.

Gene expression and histone modifications in the myometrium undergo significant changes during labor[20–23]. Histone modifications critically regulate gene expression by altering chromatin structure, thereby affecting DNA accessibility to the transcriptional machinery[24]. These dynamic modifications can distinguish one cell state from another, explaining differences between cells of the same type under varying conditions[25]. Specifically, monomethylation on lysine 4 of histone H3 (H3K4me1) marks enhancers, while trimethylation of histone H3 lysine 4 (H3K4me3) is enriched at promoters. The acetylation on lysine 27 of histone H3 (H3K27ac) and trimethylation on lysine 27 of histone H3 (H3K27me3), located at the same position at the histone tail, have opposing roles: H3K27ac maintains a loose chromatin structure that facilitates transcriptional activity and gene activation, whereas H3K27me3 compacts chromatin, inhibiting access to transcriptional machinery and thereby repressing gene expression[26,27]. H3K27ac identifies active enhancers and promoters, distinguishing them from marks like H3K4me1 or H3K4me3[28,29]. Recent advancements in chromosome conformation capture techniques, enhanced by enriching interactions via H3K27ac, have emerged as powerful tools to evaluate physical interactions among enhancers and promoters[30,31]. Enhancers are crucial regulatory elements in the genome that play key roles in controlling gene expression. Super-enhancers are composed of clusters of individual enhancers that form large regulatory regions, which are often associated with genes crucial for cell identity and function[32,33]. Previous studies on myometrial tissues from humans and mice revealed that active histone marks are present at the promoter and enhancer regions of labor-associated genes such as *GJA1*, *OXTR*, and *ZEB1*[22]. Gene expression and histone modifications also change following hypoxic stress[34,35]. We hypothesized that hypoxia in hMSMCs can induce changes in histone modifications, involving alterations in the activation of promoters and enhancers in hMSMCs. This may include the formation of enhancers or super-enhancer (SE) regions, which regulate the transcription of target genes to promote and support uterine contractions.

This study demonstrates the presence of hypoxic stress in the myometrium during labor and its promoting effect on hMSMCs contractility. Utilizing RNA-seq, histone modification ChIP-seq, and Hi-ChIP techniques, we systematically characterized the transcriptomic profiles and transcription-related histone modification (H3K27ac, H3K27me3, H3K4me3 and H3K4me1) landscapes in hMSMCs under both hypoxic and normoxic conditions, encompassing enhancer and SE regions genome-wide. Furthermore, the central regulatory role of HIF1A in mediating uterine contractions is substantiated, identifying additional HIF1A target genes in hMSMCs. This study enhances the theoretical framework of hypoxia-mediated augmentation of uterine contractions, providing insights and experimental evidence specifically related to the transcriptional regulation of labor.

Results

Hypoxia pathways are activated in the myometrium during labor

Using the bulk transcriptomics data of human myometrium from labor (TIL) and non-labor (TNL) groups, as published in our previous study (GSE181348)[20], we performed systematic pathway analysis and identified significant enrichment of hypoxia-related pathways during labor, which corroborates our earlier findings[18]. To ensure data reliability, laboring samples with prolonged labor (≥18 h) were excluded, consistent with our earlier study[20]. The final analysis involved a balanced comparison of 10 TIL samples versus 10 TNL samples. Gene set enrichment analysis (GSEA) indicated significant upregulation of hypoxia-related pathways (HARRIS HYPOXIA and REACTOME CELLULAR RESPONSE TO HYPOXIA)[36] in bulk transcriptomics data (Fig. 1a). The leading-edge genes driving hypoxia enrichment included *IGFBP1, CXCL8, HK2, SLC2A1, IL-6*, and *HIF1A* (Table S3). DEGs associated with hypoxia pathways were further identified in the bulk transcriptomics data (Fig. 1b). Among these, *SERPINE1* and *MAFF*, known to promote myometrial smooth muscle contractions[11,37,38], as well as several genes related to energy metabolism, were upregulated during labor. Spatial transcriptomics data (HRA002852) of TIL and TNL myometrium provided spatial expression information in tissue[39], showing a higher enrichment of hypoxia and cellular responses to hypoxia pathways in TIL myometrium (Fig. 1c). This observation was further validated using single-cell transcriptomics data (HRA002852) of smooth muscle cells (SMC) identified by *ACTA2*+ and *TAGLN*+ markers from TNL and TIL myometrium (Fig. 1d).

Exploration of hypoxia-induced contractions and involved pathways at the cell level

Previous multi-omics studies and functional experiments have demonstrated that hypoxia intensifies during labor and promotes myometrial contraction[7,20]. To further investigate the molecular mechanisms, in-depth studies were conducted at the cellular level using hMSMCs isolated from term pregnancy women. Two hours (h) hypoxia treatment was chosen based on observations that the contraction ability at 2 h is comparable to that at 4 and 6 h[18], with no significant differences, while cell viability begins to decline notably after 6 h (Figure S1a). It represents an early hypoxic response, enabling the capture of immediate changes in gene expression and regulatory mechanisms. The promotive effect of hypoxia on cell contraction was revalidated (Fig. 2a), confirming previously published findings[11]. Some of the hypoxia-related pathways upregulated in the myometrium during labor may not be entirely induced by hypoxia. We performed transcriptomic sequencing on hMSMCs following hypoxia induction to investigate which genes are altered due to hypoxic conditions. Concurrently, RNA-seq was conducted on the same batch of cells to investigate transcriptomic changes following hypoxia treatment. The read counts for the control group were 18,065,636, 17,109,942, and 19,210,426, while for the hypoxia group they were 18,584,773, 17,923,496, and 17,576,741. This analysis identified a total of 2,262 differentially expressed genes (DEGs), with 1,202 genes upregulated and 1,060 downregulated (Fig. 2b, Table S2). The heatmap revealed that leading-edge hypoxia-related genes identified from the GSEA results in Fig. 1a, such as *CXCL8, VEGFA, SLC2A1, HK2*, and *ENO1*, were upregulated in the hypoxia group. Pathways enriched in these DEGs include glycolysis, autophagy, and the HIF-1 pathway (Fig. 2c). GO enrichment analysis revealed upregulation in pathways associated with unfolded proteins, glucose starvation, hypoxia conditions, angiogenesis, and the TGF-beta pathway, while pathways related to protein ubiquitination, apoptosis, and GTPase signal transduction were downregulated (Fig. 2d).

Hypoxia-induced changs in histone modifications

Histone modifications play a pivotal role in regulating gene expression by modulating chromatin architecture[40]. These modifications alter the physical structure of chromatin, which in turn influences the accessibility of transcriptional machinery to DNA[41]. We performed ChIP-seq to explore the change of histone modification which involved transcriptional regulation during hypoxia. H3K27ac is linked to gene activation and is typically found near active gene promoters and enhancers[41]. In contrast, H3K27me3 marks gene repression[42]. H3K4me1 is primarily enriched at enhancers, while H3K4me3 is a key marker of active promoters, closely associated with transcriptional initiation[43]. Based on ChIP-seq data analysis of signals near genebodies, statistical analysis revealed significant differences in H3K27me3, H3K4me3, and H3K4me1 (Fig. 3a). H3K4me3 was highly enriched at transcription start sites (TSS), with an increase under hypoxia. Similarly, H3K27ac was also enriched at TSS regions, showing a modest elevation in the hypoxic condition. In contrast, H3K27me3 and H3K4me1 exhibited lower enrichment at TSS regions. Differential peak analysis revealed more differences in H3K27ac

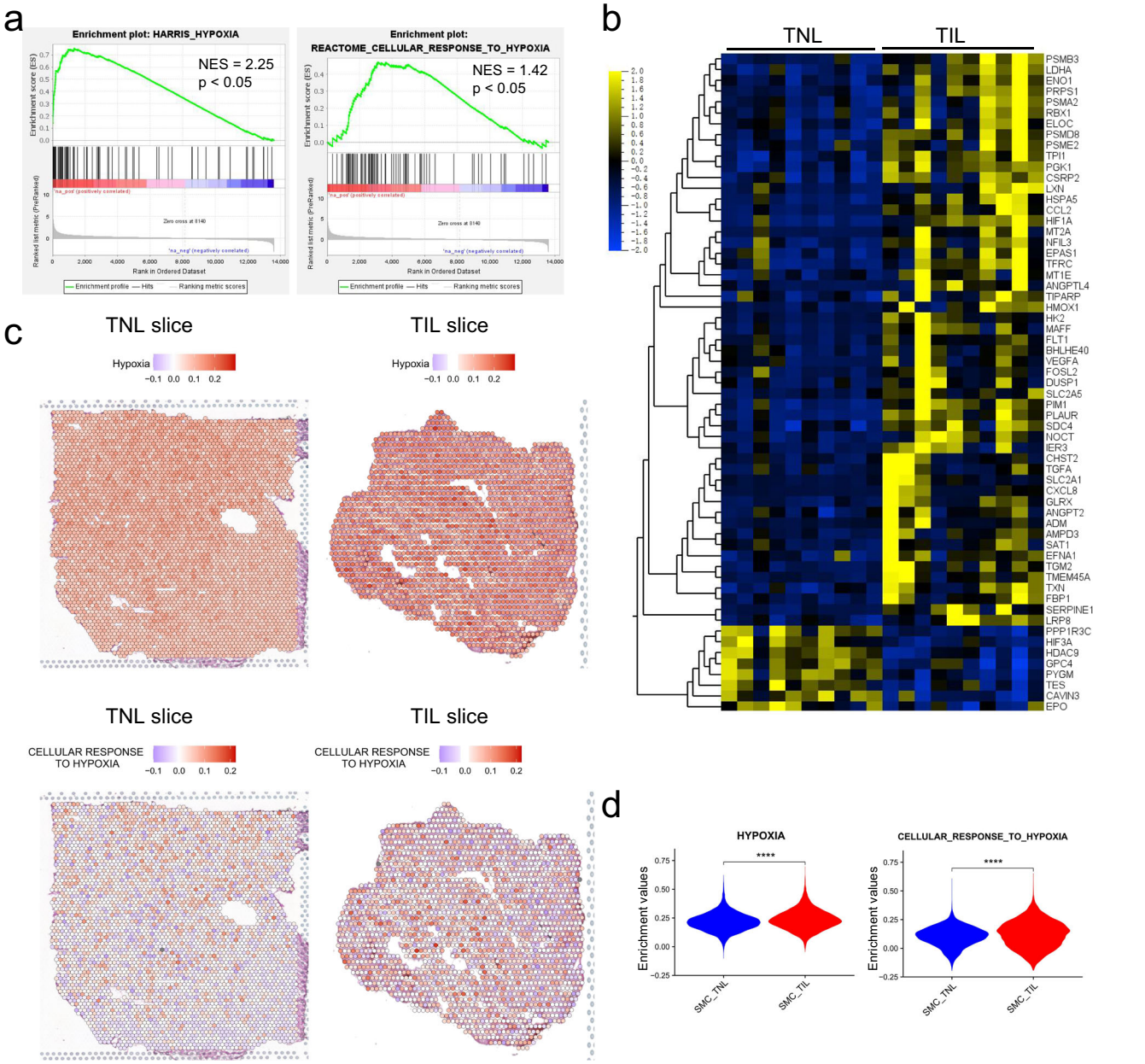

Fig. 1 | Hypoxia pathways enhanced in myometrium during labor. a GSEA showing upregulation of hypoxia-related pathways during labor (HARRIS HYPOXIA and REACTOME CELLULAR RESPONSE TO HYPOXIA) in bulk transcriptomics data of term in labor (TIL) ($n = 10$) and term in non-labor (TNL) ($n = 10$) myometrium (GEO database: GSE181348). **b** Heatmap depicting the expression of differentially expressed genes (DEGs) in the hypoxia-related pathways (combine the gene lists of HARRIS HYPOXIA, REACTOME CELLULAR RESPONSE TO HYPOXIA, and HALLMARK HYPOXIA) in TIL ($n = 10$) and TNL ($n = 10$) myometrium bulk transcriptomics data. Values are expressed as TPM (Transcripts Per Million). **c** Enrichment values of hypoxia and cellular response to hypoxia-related pathways in TIL and TNL spatial transcriptomics data (GSA database: HRA002852). Each spot, marked from red to blue, indicates the enrichment score of the pathway at the corresponding spatial location. **d** Enrichment values of hypoxia and cellular response to hypoxia-related pathways in TNL ($n = 5$) and TIL ($n = 5$) single-cell transcriptomics data of smooth muscle cells (SMC) (*ACTA2*+ and *TAGLN*+) (GSA database: HRA002852). ****$p < 0.0001$.

and H3K4me1 signals, compared with H3K27me3 and H3K4me3, suggesting that hypoxia induces more significant changes in enhancer regions (Fig. 3b, Table S4). The correlation between the hypoxia and control groups is 0.91 for H3K27ac, 1 for H3K27me3, 0.99 for H3K4me3, and 0.98 for H3K4me1 (Fig. 3c). Comparatively, hypoxia has a more significant impact on H3K27ac. Overall, even small changes in these histone modifications, which are associated with transcriptional regulation, can lead to widespread downstream gene expression changes. The relatively minor alterations observed here suggest that these modifications are sufficient to reflect adaptations to hypoxia and enhanced contractility without indicating drastic changes in cell type.

Dynamic landscape of enhancer activity under hypoxia in hMSMCs

H3K27ac serves as a biomarker for active enhancers, non-coding genomic regions that significantly boost the transcriptional activity of target genes[43]. Changes in H3K27ac levels reflect modifications in enhancer regions. Using the ROSE algorithm on H3K27ac ChIP-seq data, enhancer and SE regions were mapped under normoxic and hypoxic conditions (Fig. 4a). Hypoxic hMSMCs showed 26,019 enhancers, with 723 classified as SEs. In normoxia (Control), 29,532 enhancers were identified, including 1,263 SEs (Fig. 4b, Table S5). The number of enhancers and super-enhancers slightly decreased in hypoxia group. We analyzed the levels of H3K27ac signals on enhancers

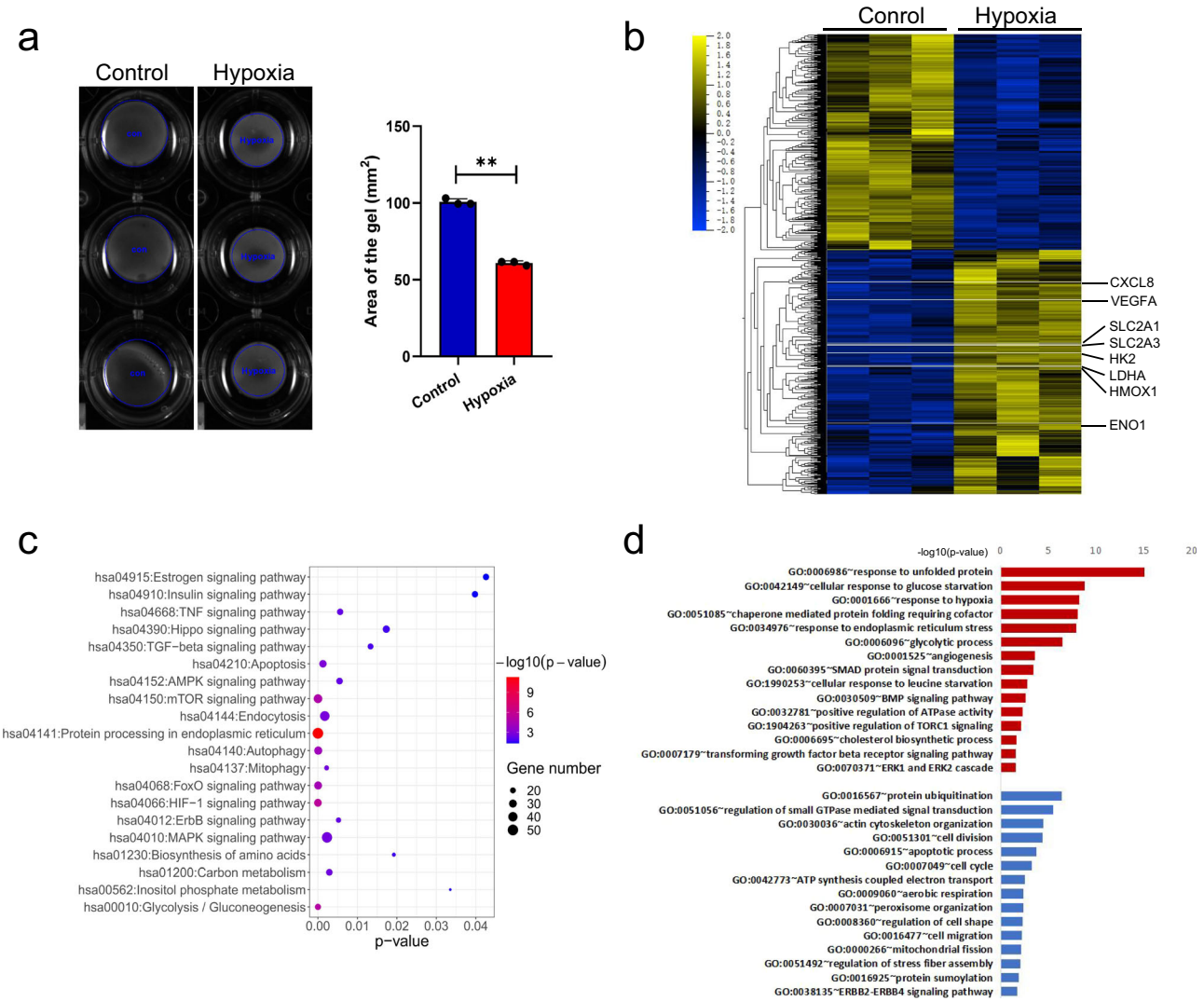

Fig. 2 | Hypoxia treatment increased the contractility of hMSMCs. a Gel contraction assay of hMSMCs with or without hypoxia treatment. $n = 3$. Data are represented as mean ± SD. $^{**}p < 0.01$. **b** Heatmap showing the expression of DEGs with or without hypoxia treatment in hMSMCs RNA-seq data. $n = 3$. Some leading-edge genes from the GSEA resultsin Fig. 1a are annotated on the right panel. Values are expressed as TPM. **c** Bubble diagram of significantly enriched pathways for DEGs of hMSMCs with or without hypoxia treatment. **d** Bar diagram of partially significantly enriched biology progress GO terms for upregulated genes (red) and downregulated (blue) genes in hMSMCs under hypoxia.

in both control and hypoxic conditions. The results indicate that the H3K27ac signals are higher under hypoxia than control (Fig. 4c). This suggests that hypoxia could primarily enhances enhancer activity, thereby promoting the transcription of target genes. We further conducted HiChIP of H3K27ac in hMSMCs under both hypoxic and control to study the interactions between enhancers and promoters (Fig. 4d). Globally, H3K27ac-mediated chromatin interactions were nearly identical between hypoxia and control. We visualized histone modifications and distant interactions surrounding the *GJA1* gene loci, known as CX43, a key regulator of myometrial contraction. The results revealed a super enhancer on the gene body of *GJA1*, with high levels of H3K4me3 and H3K27ac modifications at the 5' end and high H3K4me1 modification at the 3' end (Fig. 4e). Under hypoxia, H3K27ac peaks in the SE region were higher and broader compared to those observed under normoxia.

HIF1A is enriched and binds to regions with H3K27ac modifications in hMSMCs

To investigate the causes of increased H3K27ac modifications under hypoxia, transcription factors (TFs) predicted to bind regions with higher H3K27ac modifications were identified using the motif database. These TFs were then intersected with those highly expressed in laboring myometrium in both single-cell and bulk RNA-seq data, revealing HIF1A as expected (Fig. 5a). High expression of HIF1A in smooth muscle cells (hMSMCs) was confirmed through single-cell transcriptomics (HRA002852) (Fig. S1b). Single-cell transcriptomics and spatial data (HRA002852) further indicated higher HIF1 pathway scores during labor (Fig. S1c and S1d). A combined analysis of HIF1A and histone modification ChIP-seq data under hypoxia revealed significant enrichment of H3K27ac near HIF1A peaks, with no enrichment of H3K27me3 (Fig. 5b), suggesting that HIF1A primarily acts as an activating factor in hMSMCs. Most of the HIF1A binding regions are located on enhancers, with a smaller portion found on promoters (Fig. 5c).

HIF1A and H3K27ac modifications is closely linked in hMSMCs under hypoxia

HIF1A, a master regulator of the cellular response to hypoxia, orchestrates functions including metabolic reprogramming, angiogenesis, cell survival, migration, invasion, and inflammatory responses[44–47]. We analyzed the HIF1A-binding regions located at enhancers and promoters in hMSMCs under hypoxia and identified 4,472 genes with

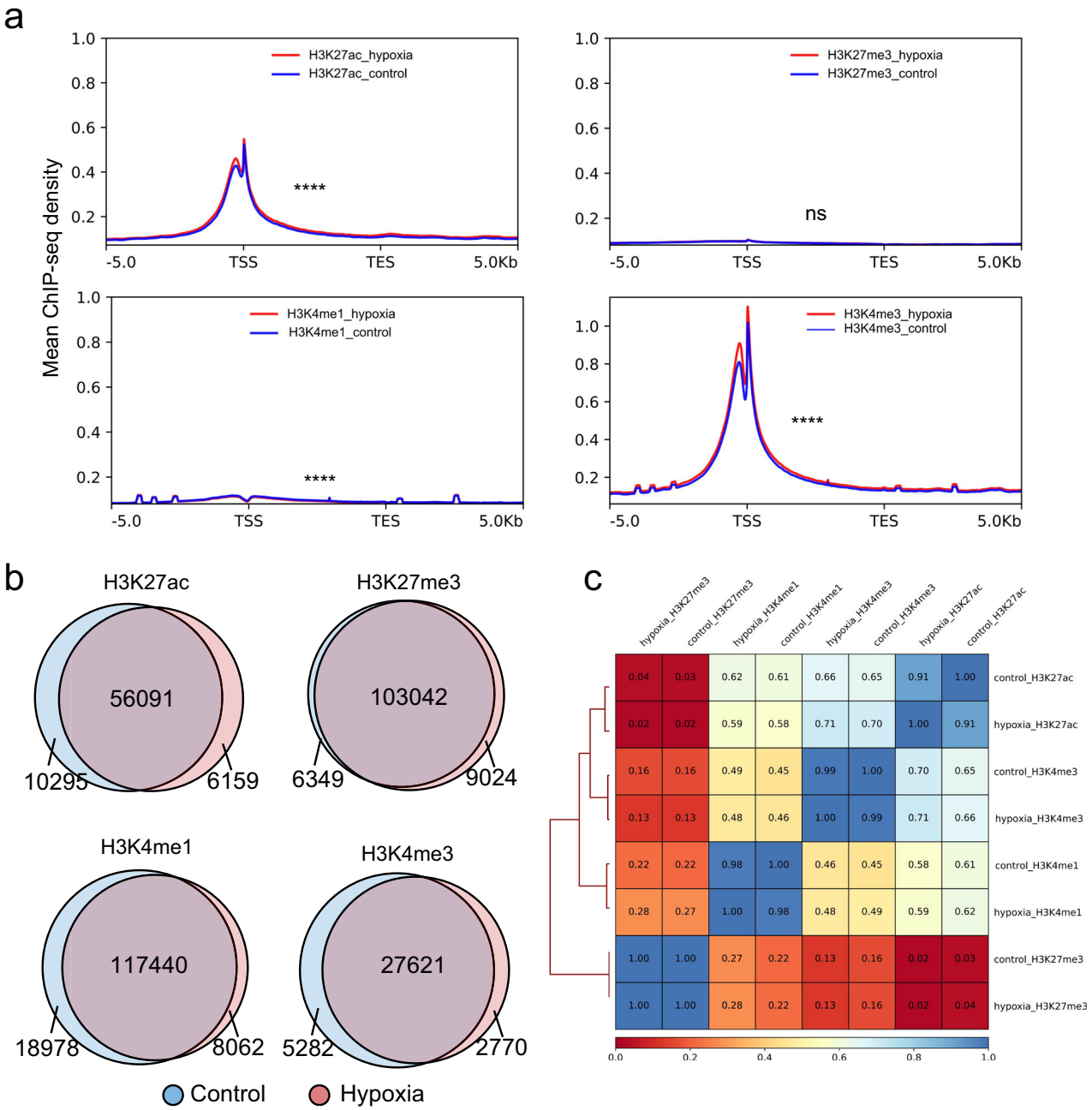

Fig. 3 | Hypoxia treatment alters histone modifications of hMSMCs. a Mean ChIP-seq density of histone modifications (H3K27ac, H3K4me1, H3K27me3, H3K4me3) at all genes' bodies (transcription start sites, TSS; transcription end sites, TES). Red line represents the hypoxia group, blue line represents the control group. Significance was determined by by two-side Wilcoxon test. ****$p < 0.0001$; ns, $p > 0.05$. **b** Venn diagram illustrating the overlap in histone modification peaks (H3K27ac, H3K4me1, H3K27me3, H3K4me3) between hypoxia and control groups. **c** Heatmap showing the correlation between different histone modifications under hypoxia or control conditions.

HIF1A binding sites nearby. These genes represent potential HIF1A targets in hMSMCs. By intersecting these genes with those upregulated under hypoxia and during labor, we found that 423 genes are highly expressed in the myometrium during labor, 456 genes are upregulated under cellular hypoxia, and 55 genes are shared between these two groups (Fig. 6a, b). To illustrate the relationship between super-enhancers, promoters, and HIF1A, we visualized the genome nearby *RUNX1*, which is well-characterized involvement in pro-inflammatory processes in the myometrium during labor[48] (Fig. 6c). SEs were located at the head and tail of the *RUNX1* gene body, and the *RUNX1* promoter interacted distantly with multiple enhancers, with HIF1A predominantly binding. Based on H3K4me3 signals, the promoter region of *RUNX1* in hMSMCs is primarily located near the transcription start sites of two shorter isoforms. The HIF1A-binding regions exhibit high levels of H3K27ac modification. IL-6, CXCL8, and other cytokines are highly expressed during labor and play pro-inflammatory roles[49]. We further analyzed the histone modifications of the *IL-6* gene (Fig. 6d). A distal HIF1A-binding site is observed near the *IL-6* gene, with long-range interactions connecting it to the *IL-6* promoter region (marked by high H3K4me3). This suggests that *IL-6* is regulated by HIF1A via distal interactions. However, hypoxia RNA-seq data indicate that IL-6 expression is not significantly upregulated under hypoxia treatment, potentially due to negative regulation by other factors.

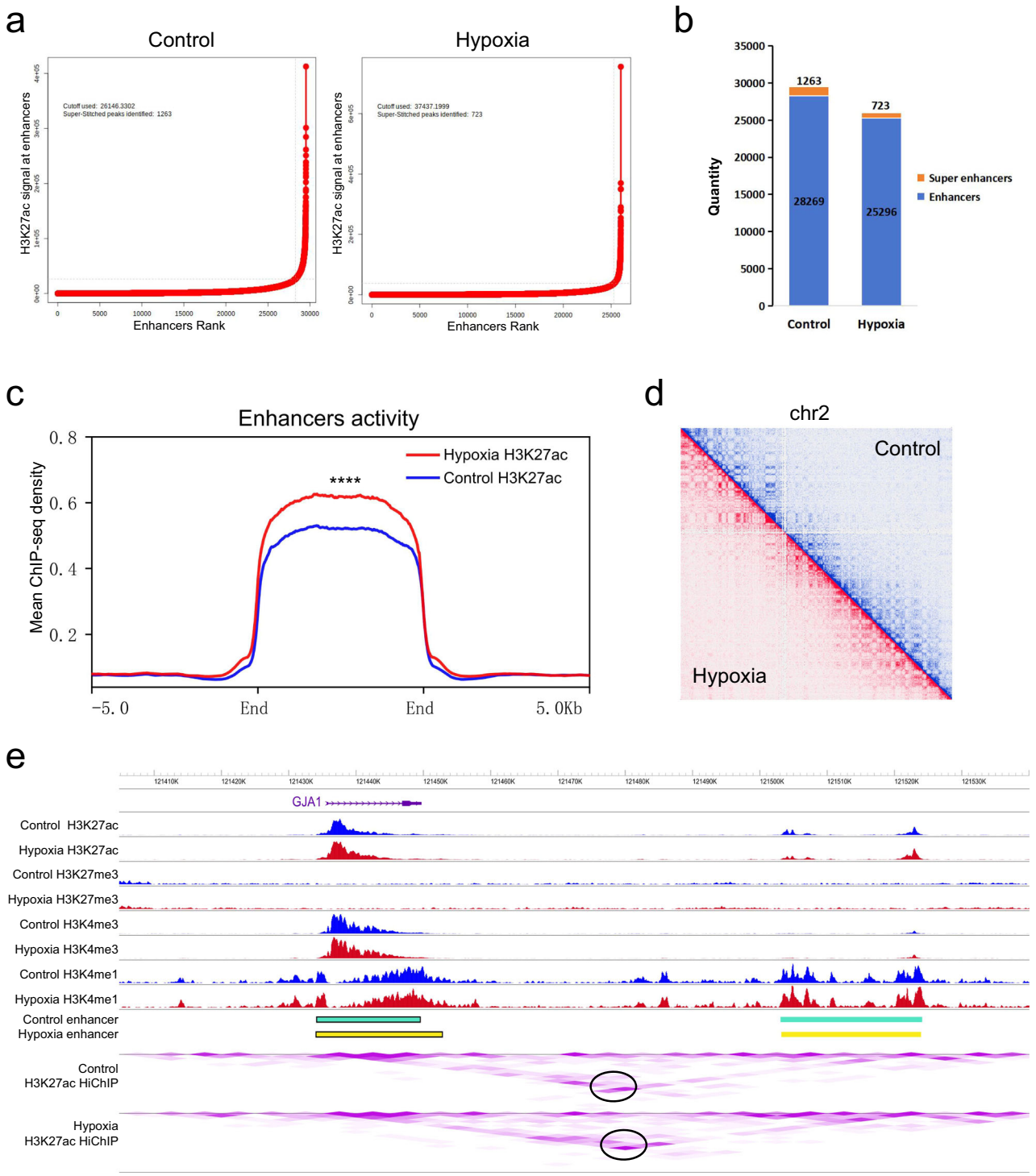

Fig. 4 | Enhancers in hMSMCs with and without hypoxia treatment. a Ranking of SEs and enhancers in hMSMCs with and without hypoxia treatment determined by H3K27ac ChIP-Seq and ROSE analysis. **b** Number of SEs and enhancers in hMSMCs under hypoxia and control conditions. **c** Mean ChIP-seq density of histone H3K27ac at all enhancers in hMSMCs with and without hypoxia treatment. The two "End" positions represent the flanking regions of the enhancer. Significance was determined by by two-side Wilcoxon test. ****$p < 0.0001$. **d** Hi-ChIP heatmaps comparison of hypoxia and control at 500 kbp resolution (balanced normalization) for chromosome 2, indicating no major changes at the high-order chromatin level in hMSMCs. **e** Profiles of SEs, H3K27ac HiChIP, and histone modifications (H3K27ac, H3K27me3, H3K4me3, and H3K4me1) ChIP-seq at the locus of the contraction-related gene GJA1 in hMSMCs under control and hypoxia. Enhancer predictions identify control enhancers (blue-green), control SEs (blue-green with a black border), and hypoxic enhancers (yellow), hypoxic SEs (yellow with a black border). Chromatin interaction data (HiChIP) visualize looping interactions under control and hypoxia conditions. The black circles indicate the interactions between promoter and distal enhancer.

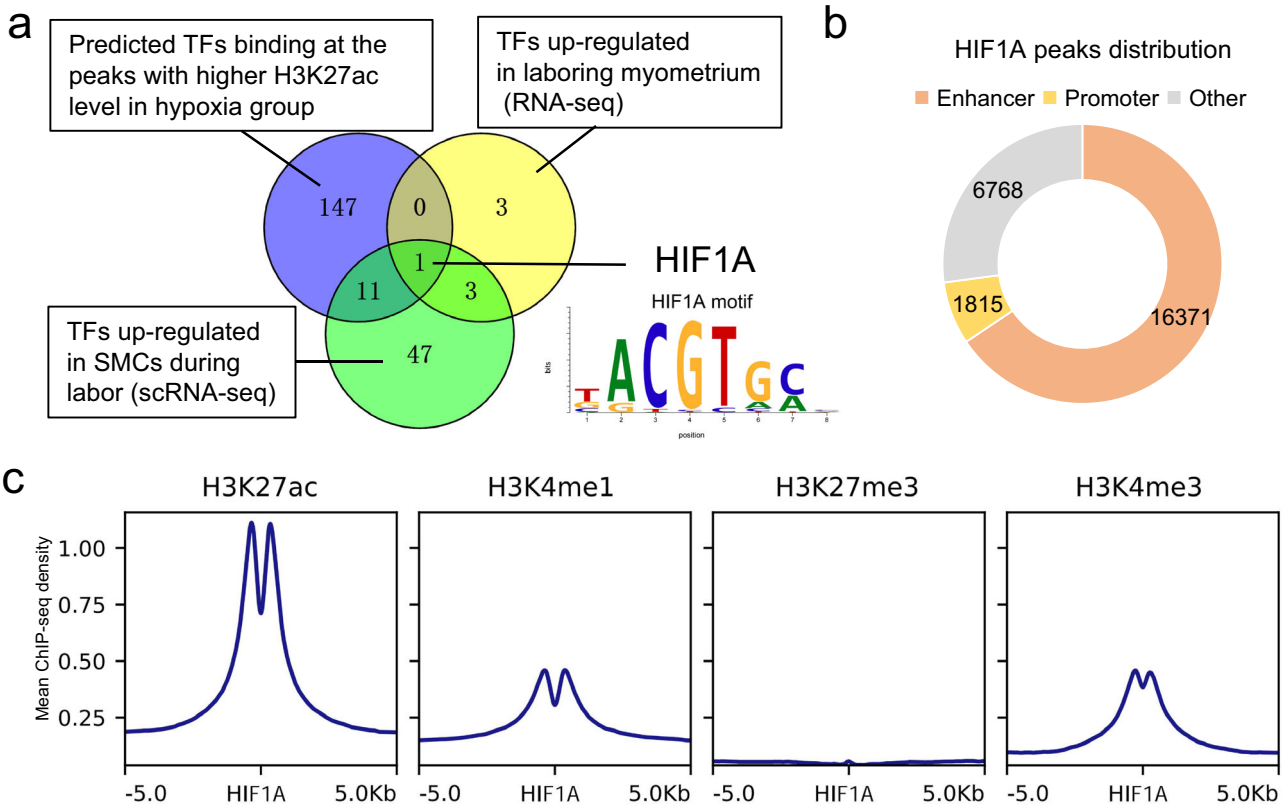

Fig. 5 | The HIF1A is enriched and specifically bind to the higher H3K27ac modifications regions in hMSMCs under hypoxia. a Predicted transcription factors (TFs) binding at the peaks with higher H3K27ac levels in the hypoxia group overlap with upregulated TFs during labor in both bulk and single-cell transcriptomics data. The lower right corner highlights HIF1A and shows its motif sequence. **b** Distribution of HIF1A peaks in promoters and enhancers in hypoxia hMSMCs. **c** Mean ChIP-seq density of histone modifications (H3K27ac, H3K4me1, H3K27me3, H3K4me3) in the hypoxia group at HIF1A ChIP-seq peaks.

Verification of HIF1A promote the expression of its targets though H3K27ac modifications

To further validate the target genes regulated by HIF1A, HIF1A was knocked down in hMSMCs using siRNA under hypoxic conditions (Fig. S1e and S1f), and we selected partial non-canonical and canonical target genes of HIF1A involved in inflammation, cell adhesion, glycolysis, and cell contraction for verification. All tested genes were downregulated in si-HIF1A hMSMCs compared to the negative control (NC) (Fig. 7a). We verified the binding of HIF1A to the enhancers or promoters of some of these genes through ChIP-qPCR (Fig. 7b). Given reports that P300 specifically binds to HIF1A as a co-activator and mediates acetylation of histone H3K27 under hypoxic conditions[50], we validated the interaction between HIF1A and P300 in hMSMCs (Fig. 7c, 7d). The level of H3K27ac modifications at HIF1A binding regions was assessed through ChIP-qPCR following HIF1A knockdown under hypoxia. H3K27ac modifications were broadly reduced, with one exception (Fig. 7e). Previous studies indicated that knocking down HIF1A in hMSMCs reduces glycolysis[11]. In this study, we observed that some HIF1A target genes upregulated during labor are involved in cell adhesion and the extracellular matrix. Notably, knockdown of HIF1A in hMSMCs led to increased cell adhesion (Fig. 7f), while prior research has reported decreased adhesion of hMSMCs during labor[51].

Discussion

Building on previous research showing hypoxia promotes myometrial contraction, this study elucidates HIF1A mediates H3K27ac histone modifications under hypoxic stress, which is associated with enhanced cell contraction. Transcriptomic and epigenetic changes in hMSMCs following hypoxia were uncovered, identifying enhancers and SEs and their roles in promoting myometrial contraction. Additionally, epigenetic modifications and long-range chromosomal interactions within hMSMCs were mapped, revealing additional genes and molecular mechanisms regulated by HIF1A. This research establishes a theoretical foundation for further studies on the regulation of myometrial contractions.

Hypoxia-strengthened uterine contractions have been validated in both humans and rats, and this study confirms these findings at the cellular level[8,11,18]. A recent study using $CoCl_2$ to simulate hypoxia reported that hypoxia promotes relaxation in hMSMCs[52]. However, this study applied a 24-h hypoxic condition, which we thought may have compromised the viability of the cells, ultimately leading to reduced contractility. Hypoxia-inducible factors (HIFs) are critical transcription factors in the cellular response to hypoxia, comprising HIF-1, HIF-2, and HIF-3, each with an alpha and a beta subunit. The beta subunit (HIF-1beta, also known as ARNT) is common to all HIFs, while the alpha subunit varies: HIF-1alpha (HIF1A), HIF-2alpha (HIF2A), and HIF-3alpha (HIF3A)[53]. Previous studies indicated that HIF1A primarily functions during labor, with high expression observed in multi-omics analyses[18]. HIF1A is associated with acute hypoxia, whereas HIF2A is involved in chronic hypoxia[54]. The integrated analysis of histone modification and transcriptomic data aligns with earlier findings, further validating HIF1A's crucial role in regulating uterine contractions during labor. Earlier research demonstrated HIF1A's regulation of contraction-associated proteins (CAPs) such as *GJA1, PTGS2*, and *OXTR*[18]. HIF1A also influences genes involved in angiogenesis (e.g., *VEGF*), glycolysis (e.g., *GLUT1, LDHA*), immune responses (e.g., *IL-6*), and cell survival (e.g., *BCL2*)[55–57]. There are few studies on HIF1A target genes in hMSMCs currently. Our previous research identified that *PTGS2*, *GJA1*, and *OXTR* are HIF1A targets. Hiroshi Ishikawa et al. verified hypoxia upregulated mRNAs of 6 potential HIF-responsive genes (*ALDOA, ENO1, LDHA, VEGFA, PFKFB3*, and *SLC2A1*), but it remains unclear whether these genes are directly or indirectly regulated by HIF1A. HIF1A has binding sites at enhancers or promoters of over 3,000 genes, all of which could be potential

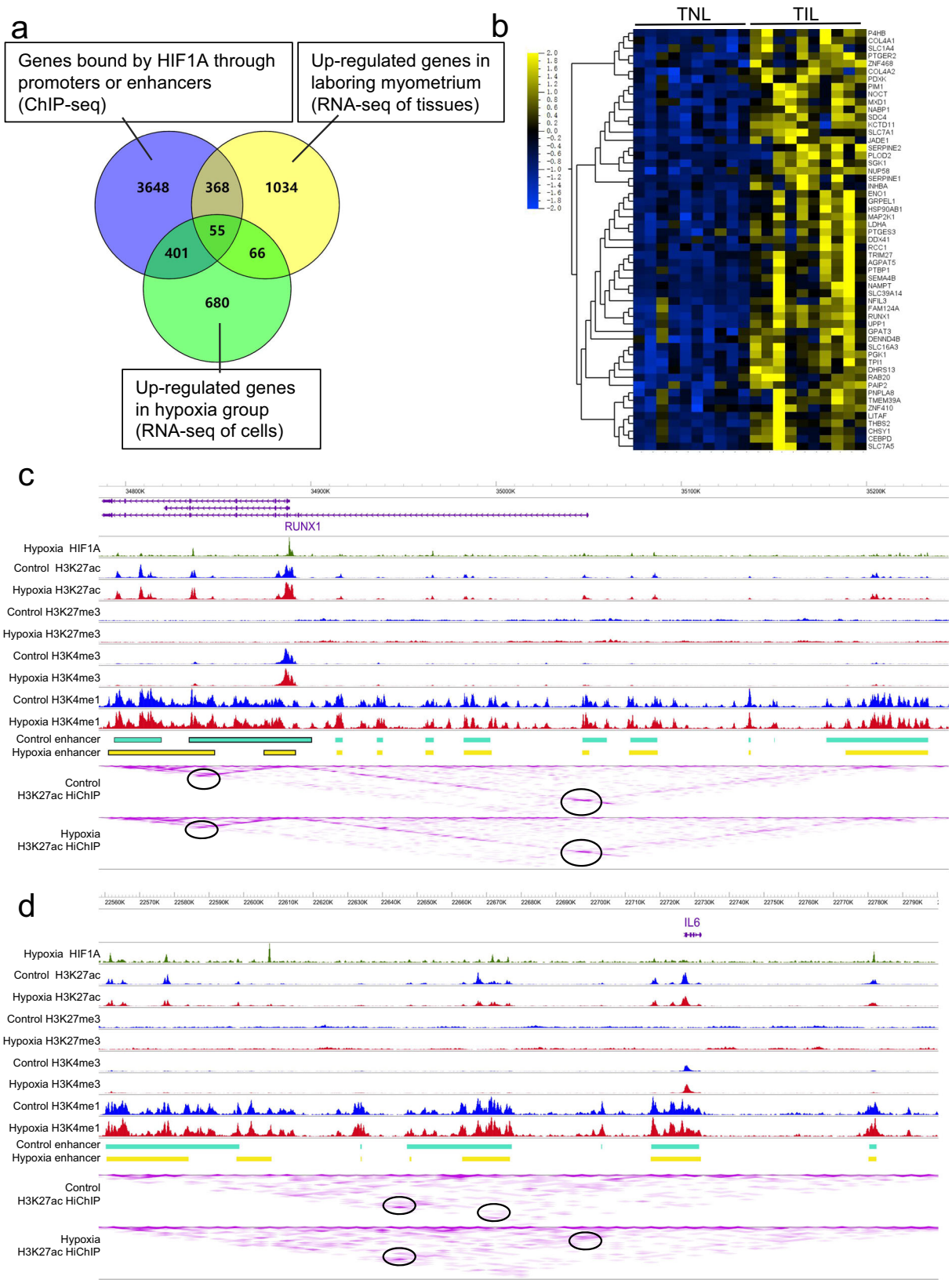

targets. Due to the large number of genes, we validated only a subset of HIF1A potential target genes that are upregulated during labor using qPCR. Additionally, we prioritized selecting genes with promoters that do not overlap with those of other genes for ChIP-qPCR validation, confirming that such as *RUNX1*, *CXCL8*, and *VDAC1* are newly identified HIF1A target genes in hMSMCs, which were previously unrecognized. These HIF1A target genes in hMSMCs are regulated through both proximal promoter interactions and distal enhancer elements. Genes highly expressed during labor were identified and experimentally validated, showing that HIF1A modulates their transcription by altering H3K27ac histone modifications.

Fig. 6 | Screening of Labor-Related Genes Regulated by HIF1A. a Venn diagram shows the overlap between genes bound by HIF1A through promoters or enhancers, genes upregulated in laboring myometrium, and genes upregulated under hypoxic conditions. **b** Heatmap depicting the expression of DEGs from Fig. 6A in bulk transcriptomics data of TNL and TIL myometrium (GEO database: GSE181348). Values are expressed as TPM. **c** Profiles of SEs, H3K27ac HiChIP, HIF1A ChIP-seq, and histone modifications (H3K27ac, H3K27me3, H3K4me3, and H3K4me1) ChIP-seq at the locus of RUNX1 in hMSMCs. Enhancer predictions identify control enhancers (blue-green), control SEs (blue-green with a black border), and hypoxic enhancers (yellow), hypoxic SEs (yellow with a black border). Chromatin interaction data (HiChIP) visualize looping interactions under control and hypoxia conditions. The black circles indicate the interactions between promoter and distal enhancer. **d** Profiles of SEs, H3K27ac HiChIP, HIF1A ChIP-seq, and histone modifications (H3K27ac, H3K27me3, H3K4me3, and H3K4me1) ChIP-seq at the locus of IL-6 in hMSMCs. Enhancer predictions identify control enhancers (blue-green) and hypoxic enhancers (yellow). Chromatin interaction data (HiChIP) visualize looping interactions under control and hypoxia conditions. The black circles indicate the interactions between promoter and distal enhancer.

These newly identified target genes present promising opportunities for managing parturition-related disorders through therapeutic approaches such as neutralizing antibodies, siRNA, or small-molecule inhibitors to regulate myometrial contraction[58–60].

Three-dimensional genome technology (HiChIP) identified genes remotely regulated by HIF1A, extending research beyond promoters and significantly increasing the number of predicted HIF1A target genes. The findings indicate that HIF1A-regulated target genes are primarily involved in metabolic processes. Previous study demonstrated that HIF1A enhances ATP production under hypoxic stress, with HIF1A knockdown resulting in oxygen consumption rates[11]. Among these target genes, many are related to the extracellular matrix (ECM) and cell adhesion. Prior research identified that HIF1A regulates the ECM-related gene SERPINE1[11], and this study additionally identified its paralog, *SERPINE2*, as a target of HIF1A. Furthermore, this study revealed that HIF1A regulates the expression of *THBS1, THBS2, LAMA1*, and *CTSL*. The ECM, encompassing mixtures of polysaccharides and proteins, including collagens, fibronectins, laminins, and proteoglycans[61,62], acts as structural and biochemical support to surrounding cells and has been suggested to regulate myometrial contraction[63–65].

Previous studies observed decreased cell adhesion in laboring hMSMCs compared to term non-labor and non-pregnant hMSMCs[51]. In this work, the adhesive capacity of hMSMCs was restored following HIF1A knockdown. These findings suggest that HIF1A may play a role in regulating uterine contractions by modulating cell adhesion. Among the adhesion-related proteins targeted by HIF1A, some, like *LAMA1*, promote adhesion, while others, like *SERPINE1/2*, inhibit it[66–68]. Changes in ECM and cell adhesion may both facilitate and coordinate myometrial contraction. The increase in lactate metabolism mediated by HIF1A under hypoxia is also crucial for the decreased adhesion of hMSMCs. In other cell types, such as tumor cells, HIF1A primarily downregulates E-cadherin and upregulates matrix metalloproteinases (e.g., *MMP2* and *MMP9*), weakening intercellular adhesion and promoting epithelial-mesenchymal transition, thus enhancing migratory and invasive abilities[69,70]. In endothelial cells, HIF1A upregulates vascular endothelial cadherin (VE-cadherin) and integrins, enhancing inter-endothelial adhesion and maintaining vascular integrity and barrier function[71,72]. In immune cells, HIF1A upregulates intercellular adhesion molecule 1 (*ICAM1*) and vascular cell adhesion molecule 1 (*VCAM1*), promoting immune cell adhesion at inflammation sites and their transmigration across the vascular wall[73,74]. In hMSMCs, HIF1A primarily mediates the expression of genes like *SERPINE1/2* that inhibit adhesion and enhances lactate production. Lactate accumulation acidifies the cellular microenvironment, which can alter the structure of adhesion molecules on the cell surface and the ECM, thereby weakening intercellular adhesion[75,76]. HIF1A regulates the expression of these genes primarily by recruiting p300, which enhances H3K27ac modifications at binding regions. This alters the chromatin structure, transforming it from a tightly packed heterochromatin state to a more relaxed euchromatin state[77]. This structural change allows transcription factors and RNA polymerase easier access to the DNA, thereby promoting gene transcription[78].

Over 20,000 enhancers and SEs were identified in hMSMCs, with the most overlapping between hypoxia and normoxia groups. The unchanged regions likely play a crucial role in maintaining the cellular characteristics of hMSMCs. Changes in enhancer and SE regions are attributed to variations in transcription factor expression induced by hypoxia. While the enrichment of HIF1A was anticipated, the potential roles of other transcription factors, such as *RUNX1* and *MAFF*, which were identified in HIF1A target gene analysis, cannot be excluded. Increased expression of these factors may enhance the transcription of their downstream genes, further strengthening contractility. This study focused on HIF1A's transcriptional regulation, yet some altered enhancer and SE regions do not show HIF1A binding, indicating additional factors are at play. We also observed that some HIF1A binding sites are located in inactive regions outside of enhancers and promoters. These regions may be in a "poised" state[79], with HIF1A binding potentially serving as a pre-marking step for future activation. Alternatively, these inactive regions could be under competitive control by other repressive factors, preventing their immediate activation. Additionally, the three-dimensional structure of chromatin may bring transcription factors into proximity with inactive regions. These regions, through chromatin looping, might be spatially adjacent to active regions, serving as temporary binding sites for transcription factors. Future research will investigate these regions, along with the unchanged enhancer and SE regions. Hormones, mechanical stress, and neural regulation may induce epigenetic modifications in these areas, warranting further exploration.

This study has limitations. Our in vitro cell experiments cannot fully replicate the complex in vivo environment during labor. The actual in vivo environment involves various hormones, exosomes, and cytokines, as well as interactions with other cell types, such as immune cells and stromal cells. Additional, our cell culture system uses normoxia (21% oxygen) as control, although is a common concentration, which may hyperoxic and mask the true physiological responses. We identified 423 HIF1A-regulated target genes with increased expression during labor through analysis. However, due to the large number of genes, not all of them were validated. We selected only a subset for experimental validation, and the contribution of some genes to uterine contractility remains unclear and requires further investigation. Additionally, the low n number of ChIP-seq and Hi-ChIP data is another limitation of this study. Moreover, while we explored the impact of HIF1A on H3K27ac modifications, its potential effects on promoter-enhancer looping were not investigated, representing a key direction for future research.

This study demonstrates that under hypoxic stress, HIF1A drives changes in histone modifications, regulating target gene expression and enhancing myometrial contraction. Transcriptomic and histone modification changes in hMSMCs post-hypoxia were revealed, highlighting the crucial role of enhancers and SEs in this process. The mapping of epigenetic modifications and long-range chromosomal interactions in hMSMCs offers a deeper understanding of the molecular mechanisms governing myometrial contraction. Furthermore, this research identifies more targets for regulating contraction, holding significant potential for precise prevention and treatment of parturition-related disorders.

Methods

hMSMCs culture

Primary hMSMCs were isolated from term pregnant women who underwent cesarean section without any complications, as described in our previous studies[11,18]. This study was approved by the ethics committee of Guangzhou Women and Children Medical Center (No. 201915401). All ethical regulations relevant to human research participants were followed. The cells were cultured in DMEM supplemented with 10% FBS, 100 U/mL of penicillin and 100 μg/mL of streptomycin (Gibco) at 37°C in a 5% CO_2

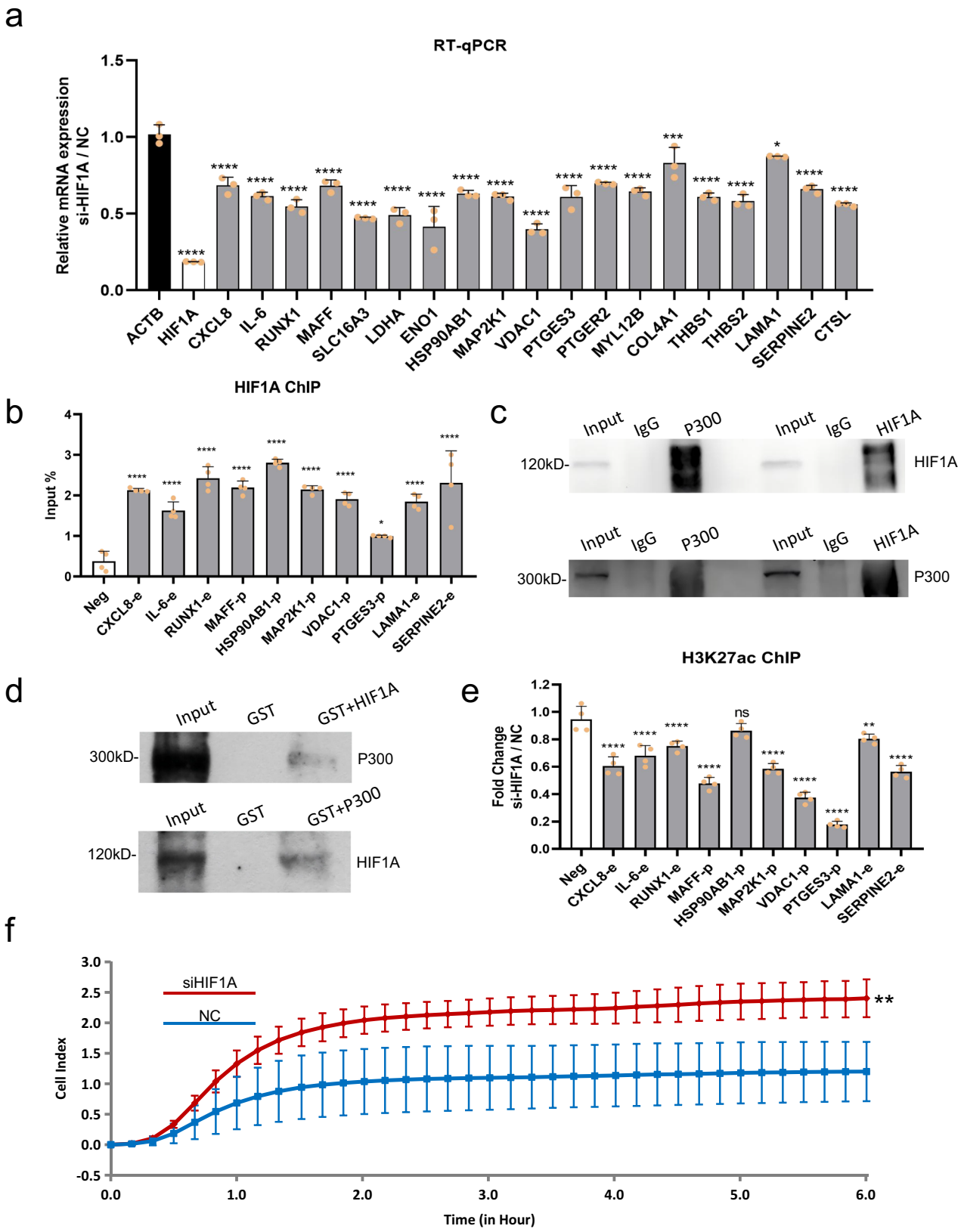

atmosphere. No exogenous progesterone, oxytocin or prostaglandins were added to the culture media. For hypoxic treatment, the hMSMCs were incubated in a Hypoxystation (Don Whitley Scientific, Yorkshire, UK) at 37°C, with 3% O_2, 5% CO_2 and 92% N_2 for 2 h, following our established protocol[11,18].

Public RNA-seq, spatial transcriptome and scRNA-seq analysis

Gene expression data from RNA-seq (GEO database: GSE181348, TNL: $n = 10$ and TIL: $n = 10$), spatial transcriptome (GSA database: HRA002852, TNL: $n = 1$ and TIL: $n = 1$) and scRNA-seq (GSA database: HRA002852, TNL: $n = 5$ and TIL: $n = 5$) of TNL and TIL myometrium were obtained

Fig. 7 | HIF1A upregulates its target genes by enhancing H3K27ac modifications at their promoters or enhancers. a RT-qPCR verification of the expression of some HIF1A target genes. $n = 3$. Data are represented as mean ± SD. *, ***, and **** indicate $p < 0.05$, $p < 0.001$, and $p < 0.0001$, respectively. **b** ChIP-qPCR verification of HIF1A binding at the promoters (suffix with "*p*") or enhancers (suffix with "*e*") of partial HIF1A target genes. $n = 4$. Data are represented as mean ± SD. A non-HIF1A peak region was set as a negative control (Neg). * and **** indicate $p > 0.05$ and *p*-value < 0.0001, respectively. **c** The interaction between HIF1A and P300 proteins was confirmed through Co-immunoprecipitation (Co-IP) followed by Western blot analysis. **d** The interaction between HIF1A and P300 proteins was validated using a GST pull-down assay followed by Western blot analysis. **e** ChIP-qPCR detection of H3K27ac modifications changes at the promoters or enhancers of partial HIF1A target genes after HIF1A knockdown. $n = 4$. Data are represented as mean ± SD. A non-HIF1A peak region was set as a negative control (Neg). ns, **, and **** indicate $p > 0.05$, $p < 0.01$, and $p < 0.0001$, separately. **f** Cell adhesive properties in si-HIF1A and negtive control (NC) hMSMCs. The y-axis represents the cell index. $n = 3$. Data are represented as mean ± SD. $^{**}p < 0.01$.

from our previous study[5,20,39]. For RNA-seq, TPM (Transcripts Per Million) values were used to generate heatmaps of the indicated genes. Analyses of spatial transcriptome and scRNA-seq data were performed using the R package Seurat (v5.1.0)[80]. Pathway module scores were calculated using the AddModuleScore function in Seurat, which computes the average expression of each gene signature list subtracted from the aggregated expression of control feature sets.

Pathways enrichment analysis

GSEA (http://software.broadinstitute.org/gsea) and DAVID (https://david.ncifcrf.gov/home.jsp,version 6.8) were used to perform Kyoto Encyclopedia of Genes and Genomes (KEGG) pathway and Gene Ontology (GO) were analyses based on the DEGs[81,82]. An adjusted P-value < 0.05 was considered indicative of strong enrichment in the annotation categories.

Cell transfection

To investigate the role of HIF1A in myometrial contractions, hMSMCs at 70%–80% confluency were transfected with either HIF1A siRNA (si-HIF1A, 10 nM) or control siRNA (si-NC, 10 nM) using INTERFERin® (Polyplus) according to the manufacturer's instructions. The sense sequences (5'-3') for si-HIF1A were: J-004018-07 (GAACAAAUACAUGGGAUUA), J-004018-08 (AGAAUGAAGUGUACCCUAA), J-004018-09 (CAAGUAGCCUCUUUGACAA), and J-004018-10 (CAAGUAGCCUCUUUGACAA). Non-targeting sequences served as controls. Cells were harvested for subsequent experiments 24–72 h post-transfection.

Cell Contraction Assay

The contractility of hMSMCs was evaluated using a cell contraction assay kit (Cell Biolabs Inc. San Diego, CA, USA). The cells were trypsinized and suspended, and the collagen solution was diluted with DMEM to a final concentration of 1.0 mg/mL. The cells-collagen mixture were added to a 24-well plate (1.5×10^5 cells/well), then incubated at 37 °C for 1 h to allow gelling. Subsequently, 1.0 mL of DMEM containing 10% FBS was added to each well. After 24 h of culture, the medium in each well was replaced, and the gels were released. The area of the floated gels was measured periodically from 1 to 4 h. Images of the gel areas were captured and digitized using the ChemiDoc XRS+ system and analyzed with ImageJ software.

Total RNA isolation and quantitative RT-PCR

Total RNA from hMSMCs was extracted and purified using the RNA-Quick purification kit (#RN001, ESscience, China). A total of 3×10^6 cells per well were lysed with 500 μL of lysis buffer, mixed with an equal volume of anhydrous ethanol, and transferred to centrifugal columns for centrifugation. After washing with wash buffer, the RNA pellet was air-dried in a biosafety cabinet and dissolved in DEPC-treated water. RNA purity (OD260/280 range: 1.9 - 2.0) was evaluated using the kaiaoK5500 Spectrophotometer (Kaiao, Beijing, China), and RNA integrity (28S/18S range: 1.9–2.3; RIN (RNA Intergrity Number): 9.3–9.5) and concentration (range: 124 - 212 ng/μL) were determined with the RNA Nano 6000 Assay Kit on the Bioanalyzer 2100 system (Agilent Technologies, CA, USA). Subsequently, 1 μg of total RNA was reverse-transcribed into cDNA using the PrimeScript RT reagent Kit (#RR047B, TaKaRa, Japan) and analyzed by qPCR using a QuantStudioTM Real-Time PCR System (Applied Biosystems) with TB Green Premix Ex Taq II (#RR820L Takara, Japan). The PCR conditions were as follows: 95°C for 10 min for PCR initial heat activation, 40 cycles of 95°C for 15 s for denaturation and combined annealing/extension at 60°C for 1 min. Beta Actin (ACTB) was used as an internal control. Data were analyzed using the $2^{-\Delta\Delta CT}$ method. Primers used to verify the expression of genes are obtained from PrimerBank or qPrimerDB database[83,84], and listed in Table S1.

RNA-seq and data processing

RNA purity (OD260/280 range: 1.9–2.1) was evaluated using the kaiaoK5500 Spectrophotometer (Kaiao, Beijing, China), and RNA integrity (28S/18S range: 1.8–2.2; RIN (RNA Intergrity Number): 9.1–9.6) and concentration (range: 80–115 ng/μL) were determined with the RNA Nano 6000 Assay Kit on the Bioanalyzer 2100 system (Agilent Technologies, CA, USA). For sequencing library preparation, 2 μg of total RNA per sample served as the input material, utilizing the NovaSeq 6000 S4 Reagent kit V1.5 for Illumina (E7530, NEB, USA). Paired-end sequencing was performed on an Illumina NovaSeq 6000 S4 platform (Annoroad Gene Technology, Beijing, China). The raw data of RNA-seq is available in the Genome Sequence Archive (GSA) repository with the accession numbers: HRA007795. RNA-seq reads were mapped to the human genome (Homo. sapiens, GRCh38) and transcriptome (Ensembl, release 84) using HISAT2 (v2.2.1) with default parameters[85]. Read counts were calculated using the featureCounts (v2.0.1)[86], assigning reads to Ensembl gene annotations (Homo sapiens, release 84). Differential expressed genes (DEGs) between the two groups were identified using DESeq2 package in R[87], with an adjusted p-value (adjP) < 0.05. KEGG pathways and Gene Ontology (GO) enrichment analyses were performed using DAVID (v6.8), with a p-value threshold of <0.05.

Chromatin immunoprecipitation

hMSMCs were harvested and cross-linked with 1% formaldehyde for 10 min, then quenched with 0.125 M glycine for 5 min. The cells were lysed in 1 mL of lysis buffer and rotated for 30 min at 4°C. The lysates were centrifuged at 2400 x g for 10 min at 4°C to isolate the nuclei. The nuclei were then suspended in digestion buffer and subjected to enzymatic shearing at 37°C for 10–15 min, producing chromatin fragments averaging 200–500 bp. The shearing reaction was stopped, and the fragmented chromatin was centrifuged at 18,000 x g for 10 min at 4°C. The supernatant was added to the ChIP reaction mix containing proteinA/G magnetic beads, ChIP IP buffer, antibody (H3K27ac: #8173, Cell signaling technology, USA; H3K27me3: #9733, Cell signaling technology, USA; H3K4me1: #5326, Cell signaling technology, USA; H3K4me3: #9751, Cell signaling technology, USA; HIF1A: #36169, Cell signaling technology, USA), protease inhibitor cocktail, and rotated at 4°C overnight. Following overnight incubation, the protein A/G magnetic beads were washed, and the chromatin was eluted in reverse cross-linking buffer and incubated at 65°C for 3 h. The ChIP DNA was treated with RNase A and proteinase K at 37°C for 30 min and purified using phenol-chloroform extraction. Finally, the purified ChIP DNA was processed for library generation using the QIAseq Ultralow Input Library Kit (QIAGEN), following the manufacturer's protocol. ChIP DNA was analyzed by qPCR. Primers were designed by Primer designing tool of NCBI and listed in Table S1. An inactive region within the RUNX1 genomic locus, devoid of HIF1A binding sites and active histone modifications and located outside the *RUNX1* coding sequence, functions as a negative control for ChIP-qPCR sites.

ChIP-seq data processing

Raw sequencing data were initially filtered using Trimmomatic (v0.36)[88]. Reads were classified as low-quality and discarded if >50% of their bases had a quality score ≤10. Adapter-contaminated reads were trimmed to remove sequences with at least a 10 bp overlap with the adapter. The resulting high-quality clean reads were used for protein binding site analysis. They were mapped to the human reference genome (GRCh38/hg38) using HISAT2 software (version 2.2.1) with default parameters. The MACS2 software (v2.1.1) was used for peak calling and differential peak analysis[89]. ChIP-seq data of HIF1A in hMSMCs wad obtained from GEO database (GSE197160, $n = 1$)[18]. The bedtools (v2.25.0) and ChIPseeker (v1.30.3) was used for peaks annotation and peak distribution analysis[90,91]. ChIP-seq data visualization was achieved with the WashU Epigenome Browser. The deeptools (v1.30.3) bamCoverage tool was used to generate bigwig files with a bin length of 50 bp[92]. The matrix was computed with a deeptools computeMatrix tool and plotted through deeptools plotProfile tool. Comparison among samples in genebodies or enhancers was performed using deepTools multiBigwigSummary tool and significance was determined by two-side Wilcoxon test using wilcox.test function in R. Pearson correlation scores calculated and hierarchically sorted using deepTools plotCorrelation tool. SE calling was performed using ROSE (v.0.1) with default parameters[33]. Raw data of ChIP-seq is available in the Genome Sequence Archive (GSA) repository with the accession numbers: HRA007832.

Motif analysis

MEME suite was used to identify motifs relatively enriched in the sequences of genomics fragments with default parameters[93]. The motif database HOMER was used for motifs discovery.

HiChIP and data processing

HiChIP was performed primarily following an established procedure[30,94]. hMSMCs were harvested and cross-linked with 1% formaldehyde for 10 min, quenched with 0.125 M glycine for 5 min, and then lysed in ice-cold lysis buffer. The lysates were centrifuged to isolate the nuclei, which were resuspended in 0.5% SDS, incubated, and quenched with Triton X-100. The chromatin was digested with DpnII enzyme (R0543, NEB, USA) for 16 h, followed by heat inactivation. After digestion, nuclei were resuspended in NEB buffer supplemented with DNA polymerase 1, Large (Klenow) fragment (NEB, M0210) to fill in the restriction fragment overhangs with biotin labeled dATP for 1 h. DNA was then ligated for 4 h at room temperature using T4 DNA ligase (M0202, NEB, USA). Nuclei were pelleted, and the DNA was sheared to 200–500 bp fragments with sonicator. The nuclear pellet was lysed in nuclear lysis buffer (50 mM Tris-HCl pH 7.5, 10 mM EDTA, 1% SDS, 1× protease inhibitor) and the supernatant was incubated overnight with a ChIP reaction mix containing protein A/G magnetic beads, ChIP IP buffer, antibody, and protease inhibitors. The beads were washed, and the chromatin was eluted in reverse cross-linking buffer, followed by treatment with RNase A and proteinase K, phenol-chloroform purification, and library preparation using the QIAseq Ultralow Input Library Kit (QIAGEN) according to the manufacturer's instructions. Raw data of HiChIP is available in the Genome Sequence Archive (GSA) repository with the accession numbers: HRA007796. Raw data from HiChIP experiments were processed using the HiC-Pro (v2.11.1) pipeline with Bowtie2 (v2.3.5.1) for mapping reads to human reference genome (GRCh38/hg38)[95,96]. Normalized contact matrices were then generated at resolutions of 2 kb–10KB. To visualize the chromatin interaction data, "all.validpair" files produced by HiC-Pro were converted into ".hic" files, which were visualized using Juicebox (v1.11.08) and WashU Epigenome Browser (http://epigenomegateway.wustl.edu/)[97,98].

Real-time cell adhesion assay

Experiments were conducted utilizing the S16 xCELLigence instrument (Agilent Technologies) as previously described[51]. This instrument measures cell adherence to the well bottom via microelectronic biosensors, translating signals into a relative cell index. The instrument was housed in a humidified incubator maintained at 37°C with 5% CO_2. For adhesion assays, control and conditioned cells were seeded in 16 plates at 5000 cells/well in medium containing 10% FBS. Cell adherence was monitored every 10 min for 6 h to evaluate adhesive capacity. Data were acquired using RTCA software Version 1.2 and exported for statistical analysis. The assay system quantifies impedance using arbitrary Cell Index units. At each time point, the Cell Index (CI) is calculated as $(R_n\text{-}R_b) / 15$, where R_n represents the impedance of the well containing cells, and R_b is the background impedance of the well with media alone. The value 15 serves as a normalization constant for standardization, as stated in the Application Note of xCELLigence instrument (https://www.agilent.com/en/solutions/cell-analysis/cancer-biology/real-time-cell-adhesion).

Western blotting (WB)

Cells were homogenized and lysed using ice-cold RIPA buffer (P0013, Beyotime). After centrifugation at 12,000 rpm (15,294 g) for 5 min at 4°C, the supernatant was collected. Protein concentrations were determined using the BCA assay kit (Thermo Scientific, USA). Proteins were separated by SDS-polyacrylamide gel electrophoresis (SDS-PAGE), transferred onto polyvinylidene fluoride (PVDF) membranes (Millipore, Darmstadt, Germany), and incubated with primary and secondary antibodies. Protein bands were visualized and quantified using the ChemiDoc XRS+ imaging system and ImageJ software, with β-actin serving as a loading control. The following antibodies were used: rabbit polyclonal β-actin antibody (1:5000, ab8226, Abcam), rabbit polyclonal HIF-1α antibody (1:1000, ab2185, Abcam). Protein band intensities from the precipitate were quantified using the ChemiDoc XRS+ system and lmageJ software.

Immunofluorescence

hMSMCs were fixed in 4% paraformaldehyde for 30 min and permeabilized with PBST (0.3% Triton X in PBS) for 15 min. After blocking with 10% goat serum at room temperature for 1 h, the cells were incubated overnight at 4°C with anti-α-SMA (1:500, ab7817, Abcam), anti-HIF-1α (1:500, #36169, CST). This was followed by a 1 h incubation with secondary antibodies, either Alexa 594 goat anti-mouse (1:250, ab150116, Abcam) or Alexa Fluor 488 goat anti-rabbit IgG (1:500, ab150077, Abcam). The cells were counterstained with DAPI and observed using a Leica DMi8 fluorescence microscope.

Cell viability assay

Cells were seeded at a density of 6000 cells/well in 96-well plates containing 100 μL of the medium. Cell viability of the 6,000 cells/well, incubated in hypoxia, was assessed at 0, 2, 4 and 6 h. Cells were incubated with 100 μL cell culture medium and 10 μL of CCK8 kit (SX538, DOJINDO) at 37 °C with the CCK8 kit protocol. Absorbance was read at 450 nm using a Multiskan GO (Thermo).

Co-immunoprecipitation

Cells were lysed using ice-cold cell lysis buffer (PO013,Beyotime). After centrifugation at 14,000 rpm (20,817 g) for 30 min at 4°C, the supernatant was isolated. Magnetic beads (25 μL) were added to an EP tube, separated using a magnetic holder, and the supernatant was removed. To remove specific proteins, 25 μL of beads were added to 500 μL of lysed cells and rotated at 4°C for 2 h. The supernatants were then immunoprecipitated using either rabbit monoclonal HIF1A antibody(1:50, #36169, CST), P300 antibody (1:50, #86377, CST) or rabbit monoclonal lgG antibody (1:150,#3900, Abcam) by rotating at 4°C for 5 h. After overnight incubation with antibodies, magnetic beads were added at 4°C for 2 h, followed by washing and removal of the supernatant. WB was performed to detected the protein in supernatant and protein band intensities were detected using the film development system and lmageJ software.

GST pulldown

The E. coli BL21 (DE3) were transformed with plasmid pGEX-6p-1 or pGEX-4T-2-HIF1A or pGEX-4T-2-P300 and induced to express GST or GST-HIF1A or GST-P300 proteins. The proteins were processed using a GST Protein Interaction Pull-Down Kit (#21516, Thermo Fisher Scientific) according to the manufacturer's instructions. Briefly, the GST fusion proteins were purified by GST-agarose resins (#21516, Thermo Fisher Scientific). The resins were washed and then co-incubated with hMSMCs lysates containing HIF1A or P300 at 4°C for 12 h. After washing by elution buffer, the eluted proteins were subjected to WB with HIF1A antibody (1:50, #36169, CST) or P300 antibody.

Statistics and reproducibility

Statistical analyses of gel contraction, cell viability, cell adhesion, RT-qPCR and ChIP-qPCR data were conducted using GraphPad Prism 8.0 software. Results are presented as means ± SD. The number of independent experiments, sample sizes, and details of statistical methods are provided in the figure legends. For the gel contraction, cell viability, ChIP-qPCR and RT-qPCR we used a *t*-test for comparisons between two groups. Cell adhesion assay data were analyzed using two-way ANOVA. Statistical tests used in ChIP-seq data comparison were determined by two-side Wilcoxon test using wilcox.test function in R. The Wilcoxon test was used for comparing pathway module scores between two groups using Seurat. *P*-values <0.05 were considered significant. Significance levels are indicated as follows: ns ($p > 0.05$), $^{*}p < 0.05$), $^{**}p < 0.01$, $^{***}p < 0.001$, and $^{****}p < 0.0001$.

Reporting summary

Further information on research design is available in the Nature Portfolio Reporting Summary linked to this article.

Data availability

Raw data of RNA-seq, ChIP-seq, HiChIP is available in the Genome Sequence Archive (GSA) repository with the accession numbers: HRA007795, HRA007832 and HRA007796. The source data behind the graphs in the paper is exhibited in Supplementary Data 1. Supplementary tables (S1-S5) are stored in figshare (https://doi.org/10.6084/m9.figshare.28366232.v1) (https://figshare.com/s/a3c2cceacab01e32b4c1). Uncropped blot images and Supplementary Figs. (Fig. S1) are available in the Supplementary Information. Additional requests for data and methods are available upon reasonable request to the corresponding author.

Code availability

This article contains no original code. The codes used in this article are referred the manual of each software.

Received: 7 August 2024; Accepted: 3 March 2025;
Published online: 21 March 2025

References

1. Wray, S. & Prendergast, C. The myometrium: from excitation to cntractions and labour. *Adv. Exp. Med. Biol.* **1124**, 233–263 (2019).
2. Koutras, A. et al. Physiology and pathology of contractility of the myometrium. *Vivo* **35**, 1401–1408 (2021).
3. Rosen, H. & Yogev, Y. Assessment of uterine contractions in labor and delivery. *Am. J. Obstet. Gynecol.* **228**, S1209–S1221 (2023).
4. Zierden, H. C., Shapiro, R. L., DeLong, K., Carter, D. M. & Ensign, L. M. Next generation strategies for preventing preterm birth. *Adv. Drug Deliv. Rev.* **174**, 190–209 (2021).
5. Ji, K. et al. Integrating single-cell RNA sequencing with spatial transcriptomics reveals an immune landscape of human myometrium during labour. *Clin. Transl. Med.* **13**, e1234 (2023).
6. Deng, W. et al. Proteomic and miRNA profiles of exosomes derived from myometrial tissue in laboring women. *Int. J. Mol. Sci*. **23**, 12343 (2022).
7. Chen, L. et al. Time course analysis of transcriptome in human myometrium depending on labor duration and correlating with postpartum blood loss. *Front. Genet.* **13**, 812105 (2022).
8. Alotaibi, M., Arrowsmith, S. & Wray, S. Hypoxia-induced force increase (HIFI) is a novel mechanism underlying the strengthening of labor contractions, produced by hypoxic stresses. *Proc. Natl. Acad. Sci. USA* **112**, 9763–9768 (2015).
9. Wray, S., Alruwaili, M. & Prendergast, C. HYPOXIA AND REPRODUCTIVE HEALTH: hypoxia and labour. *Reproduction* **161**, F67–F80 (2021).
10. Wen, B. et al. HIF-1alpha is essential for the augmentation of myometrial contractility during labordagger. *Biol. Reprod.* **107**, 1540–1550 (2022).
11. Wang, X. et al. Serpin family E member 1 enhances myometrium contractility by increasing ATP production during labor. *Faseb J.* **38**, e23368 (2024).
12. Ziello, J. E., Jovin, I. S. & Huang, Y. Hypoxia-Inducible Factor (HIF)-1 regulatory pathway and its potential for therapeutic intervention in malignancy and ischemia. *Yale J. Biol. Med.* **80**, 51–60 (2007).
13. Harrison, H., Pegg, H. J., Thompson, J., Bates, C. & Shore, P. HIF1-alpha expressing cells induce a hypoxic-like response in neighbouring cancer cells. *Bmc Cancer* **18**, 674 (2018).
14. Strowitzki, M. J., Cummins, E. P. & Taylor, C. T. Protein hydroxylation by hypoxia-inducible factor (HIF) hydroxylases: unique or ubiquitous? *Cells* **8**, 5 (2019).
15. Xiong, G. et al. Collagen prolyl 4-hydroxylase 1 is essential for HIF-1alpha stabilization and TNBC chemoresistance. *Nat. Commun.* **9**, 4456 (2018).
16. Mittal, P. et al. A molecular signature of an arrest of descent in human parturition. *Am. J. Obstet. Gynecol.* **204**, 115–177 (2011).
17. Chaemsaithong, P. et al. Characterization of the myometrial transcriptome in women with an arrest of dilatation during labor. *J. Perinat. Med.* **41**, 665–681 (2013).
18. Wen, B. et al. HIF-1alpha is essential for the augmentation of myometrial contractility during labor. *Biol. Reprod.* **107**, 6 (2022).
19. Lum, J. J. et al. The transcription factor HIF-1alpha plays a critical role in the growth factor-dependent regulation of both aerobic and anaerobic glycolysis. *Genes Dev.* **21**, 1037–1049 (2007).
20. Chen, L. et al. Integrated proteotranscriptomics of human myometrium in labor landscape reveals the increased molecular asociated with inflammation under hypoxia stress. *Front. Immunol.* **12**, 722816 (2021).
21. Shchuka, V. M. et al. The pregnant myometrium is epigenetically activated at contractility-driving gene loci prior to the onset of labor in mice. *Plos. Biol.* **18**, e3000710 (2020).
22. Dotts, A. J. et al. In vivo genome-wide PGR binding in pregnant human myometrium identifies potential regulators of labor. *Reprod. Sci.* **30**, 544–559 (2023).
23. Wang, W. et al. Integrating transcriptomic and ChIP-seq reveals important regulatory regions modulating gene Expression in myometrium during implantation in pigs. *Biomolecules* **13**, 1 (2022).
24. Xu, R., Li, C., Liu, X. & Gao, S. Insights into epigenetic patterns in mammalian early embryos. *Protein Cell* **12**, 7–28 (2021).
25. Zentner, G. E. & Henikoff, S. Regulation of nucleosome dynamics by histone modifications. *Nat. Struct. Mol. Biol.* **20**, 259–266 (2013).
26. Yao, J., Chen, J., Li, L. Y. & Wu, M. Epigenetic plasticity of enhancers in cancer. *Transcr. -Austin* **11**, 26–36 (2020).
27. Sankar, A. et al. Histone editing elucidates the functional roles of H3K27 methylation and acetylation in mammals. *Nat. Genet* **54**, 754–760 (2022).
28. Zhang, W., Song, M., Qu, J. & Liu, G. H. Epigenetic modifications in cardiovascular aging and diseases. *Circ. Res.* **123**, 773–786 (2018).
29. Tessarz, P. & Kouzarides, T. Histone core modifications regulating nucleosome structure and dynamics. *Nat. Rev. Mol. Cell Biol.* **15**, 703–708 (2014).

30. Mumbach, M. R. et al. HiChIP: efficient and sensitive analysis of protein-directed genome architecture. *Nat. Methods* **13**, 919–922 (2016).
31. Zhou, P. et al. Dynamic changes in P300 enhancers and enhancer-promoter contacts control mouse cardiomyocyte maturation. *Dev. Cell.* **58**, 898–914 (2023).
32. Hnisz, D., Shrinivas, K., Young, R. A., Chakraborty, A. K. & Sharp, P. A. A phase separation model for transcriptional control. *Cell* **169**, 13–23 (2017).
33. Whyte, W. A. et al. Master transcription factors and mediator establish super-enhancers at key cell identity genes. *Cell* **153**, 307–319 (2013).
34. Udayasuryan, B. et al. Fusobacterium nucleatum infection modulates the transcriptome and epigenome of HCT116 colorectal cancer cells in an oxygen-dependent manner. *Commun. Biol.* **7**, 551 (2024).
35. Tiana, M. et al. The SIN3A histone deacetylase complex is required for a complete transcriptional response to hypoxia. *Nucleic Acids Res.* **46**, 120–133 (2018).
36. Liberzon, A. et al. Molecular signatures database (MSigDB) 3.0. *Bioinformatics* **27**, 1739–1740 (2011).
37. Massrieh, W. et al. Regulation of the MAFF transcription factor by proinflammatory cytokines in myometrial cells. *Biol. Reprod.* **74**, 699–705 (2006).
38. Kimura, T. et al. Molecular cloning of a human MafF homologue, which specifically binds to the oxytocin receptor gene in term myometrium. *Biochem. Biophys. Res. Commun.* **264**, 86–92 (1999).
39. Ji, K. et al. Single-cell and spatial transcriptomics reveal alterations in trophoblasts at invasion sites and disturbed myometrial immune microenvironment in placenta accreta spectrum disorders. *Biomark. Res.* **12**, 55 (2024).
40. Kang, H. et al. Dynamic regulation of histone modifications and long-range chromosomal interactions during postmitotic transcriptional reactivation. *Genes Dev.* **34**, 913–930 (2020).
41. Zhang, Y. et al. Overview of histone modification. *Adv. Exp. Med. Biol.* **1283**, 1–16 (2021).
42. Wiles, E. T. & Selker, E. U. H3K27 methylation: a promiscuous repressive chromatin mark. *Curr. Opin. Genet. Dev.* **43**, 31–37 (2017).
43. Barral, A. & Dejardin, J. The chromatin signatures of enhancers and their dynamic regulation. *Nucleus* **14**, 2160551 (2023).
44. Cowman, S. J. & Koh, M. Y. Revisiting the HIF switch in the tumor and its immune microenvironment. *Trends Cancer* **8**, 28–42 (2022).
45. Zheng, J. et al. HIF-1alpha in myocardial ischemia-reperfusion injury (Review). *Mol. Med. Rep.* **23**, 5 (2021).
46. Rashid, M. et al. Up-down regulation of HIF-1alpha in cancer progression. *Gene* **798**, 145796 (2021).
47. Anam et al. meta-analysis of hypoxia inducible factor 1-alpha (HIF1A) gene polymorphisms: association with cancers. *Biomark. Res.* **3**, 29 (2015).
48. Lappas, M. Runt-related transcription factor 1 (RUNX1) deficiency attenuates inflammation-induced pro-inflammatory and pro-labour mediators in myometrium. *Mol. Cell. Endocrinol.* **473**, 61–71 (2018).
49. Huang, Q. et al. Elevated inflammatory mediators from the maternal-fetal interface to fetal circulation during labor. *Cytokine* **148**, 155707 (2021).
50. Yfantis, A. et al. Transcriptional response to hypoxia: the role of HIF-1-associated co-regulators. *Cells* **12**, 5 (2023).
51. Bao, J. et al. Upregulated TIMP1 facilitates and coordinates myometrial contraction by decreasing collagens and cell adhesive capacity during human labor. *Mol. Hum. Reprod.* **29**, 10 (2023).
52. Li, T. et al. High glucose induced HIF-1alpha/TREK1 expression and myometrium relaxation during pregnancy. *Front. Endocrinol.* **14**, 1115619 (2023).
53. Lee, P., Chandel, N. S. & Simon, M. C. Cellular adaptation to hypoxia through hypoxia inducible factors and beyond. *Nat. Rev. Mol. Cell Biol.* **21**, 268–283 (2020).
54. Wu, Q. et al. Hypoxia-inducible factors: master regulators of hypoxic tumor immune escape. *J. Hematol. Oncol.* **15**, 77 (2022).
55. Reece, K. M. et al. Epidithiodiketopiperazines (ETPs) exhibit in vitro antiangiogenic and in vivo antitumor activity by disrupting the HIF-1alpha/p300 complex in a preclinical model of prostate cancer. *Mol. Cancer* **13**, 91 (2014).
56. He, R. et al. HIF1A Alleviates compression-induced apoptosis of nucleus pulposus derived stem cells via upregulating autophagy. *Autophagy* **17**, 3338–3360 (2021).
57. Fan, C. et al. Hypoxia-inducible factor-1alpha regulates the interleukin-6 production by B cells in rheumatoid arthritis. *Clin. Transl. Immunol.* **12**, e1447 (2023).
58. Eltarhoni, K., Kamel, F., Ihebunezie, K., Nisar, P. & Soloviev, M. Therapeutic antibodies in cancer treatment in the UK. *Int. J. Mol. Sci.* **23**, 23 (2022).
59. Alshaer, W. et al. siRNA: Mechanism of action, challenges, and therapeutic approaches. *Eur. J. Pharmacol.* **905**, 174178 (2021).
60. Wang, J., Tomlinson, B. & Lazarus, H. M. Update on small molecule targeted therapies for acute myeloid leukemia. *Curr. Treat. Options Oncol.* **24**, 770–801 (2023).
61. Karamanos, N. K. et al. A guide to the composition and functions of the extracellular matrix. *Febs J.* **288**, 6850–6912 (2021).
62. Doyle, A. D., Nazari, S. S. & Yamada, K. M. Cell-extracellular matrix dynamics. *Phys. Biol.* **19**, 021002 (2022).
63. Lombardi, A. et al. Expression of matrix metalloproteinases in the mouse uterus and human myometrium during pregnancy, labor, and preterm labor. *Reprod. Sci.* **25**, 938–949 (2018).
64. Fan, Y. et al. Peptidomics analysis of myometrium tissues in term labor compared with term nonlabor. *J. Cell. Biochem.* **121**, 1890–1900 (2020).
65. Ouellette, A., Mahendroo, M. & Nallasamy, S. Collagen and elastic fiber remodeling in the pregnant mouse myometriumdagger. *Biol. Reprod.* **107**, 741–751 (2022).
66. Islam, K. et al. Upregulated LAMA3 modulates proliferation, adhesion, migration and epithelial-to-mesenchymal transition of cholangiocarcinoma cells. *Sci. Rep.* **13**, 22598 (2023).
67. Polo-Generelo, S. et al. Serpine1 mRNA confers mesenchymal characteristics to the cell and promotes CD8+ T cells exclusion from colon adenocarcinomas. *Cell Death Discov.* **10**, 116 (2024).
68. Wu, S. et al. Serpin peptidase inhibitor, clade E, member 2 in physiology and pathology: recent advancements. *Front. Mol. Biosci.* **11**, 1334931 (2024).
69. Chellini, F. et al. HIF-1alpha/MMP-9 axis is required in the early phases of skeletal myoblast differentiation under normoxia condition in vitro. *Cells* **12**, 24 (2023).
70. Li, G. et al. Interleukin-17A promotes rheumatoid arthritis synoviocytes migration and invasion under hypoxia by increasing MMP2 and MMP9 expression through NF-kappaB/HIF-1alpha pathway. *Mol. Immunol.* **53**, 227–236 (2013).
71. Jiang, W. et al. HIF-1alpha enhances vascular endothelial cell permeability through degradation and translocation of vascular endothelial cadherin and claudin-5 in rats with burn injury. *J. Burn Care Res.* **42**, 258–268 (2021).
72. Tang, N. N. et al. HIF-1alpha induces VE-cadherin expression and modulates vasculogenic mimicry in esophageal carcinoma cells. *World J. Gastroenterol.* **20**, 17894–17904 (2014).
73. Winning, S., Splettstoesser, F., Fandrey, J. & Frede, S. Acute hypoxia induces HIF-independent monocyte adhesion to endothelial cells through increased intercellular adhesion molecule-1 expression: the role of hypoxic inhibition of prolyl hydroxylase activity for the induction of NF-kappa B. *J. Immunol.* **185**, 1786–1793 (2010).
74. Harris, A. J., Thompson, A. R., Whyte, M. K. & Walmsley, S. R. HIF-mediated innate immune responses: cell signaling and therapeutic implications. *Hypoxia* **2**, 47–58 (2014).

75. Han, X. et al. Lactate-mediated Fascin protrusions promote cell adhesion and migration in cervical cancer. *Theranostics* **13**, 2368–2383 (2023).
76. Sousa, B., Pereira, J. & Paredes, J. The crosstalk between cell adhesion and cancer metabolism. *Int. J. Mol. Sci.* **20**, 8 (2019).
77. Wu, D. et al. A novel function of novobiocin: disrupting the interaction of HIF 1alpha and p300/CBP through direct binding to the HIF1alpha C-terminal activation domain. *Plos One* **8**, e62014 (2013).
78. Freedman, S. J. et al. Structural basis for recruitment of CBP/p300 by hypoxia-inducible factor-1 alpha. *Proc. Natl Acad. Sci. USA* **99**, 5367–5372 (2002).
79. Crispatzu, G. et al. The chromatin, topological and regulatory properties of pluripotency-associated poised enhancers are conserved in vivo. *Nat. Commun.* **12**, 4344 (2021).
80. Hao, Y. et al. Dictionary learning for integrative, multimodal and scalable single-cell analysis. *Nat. Biotechnol.* **42**, 293–304 (2024).
81. Subramanian, A. et al. Gene set enrichment analysis: a knowledge-based approach for interpreting genome-wide expression profiles. *Proc. Natl. Acad. Sci. USA* **102**, 15545–15550 (2005).
82. Huang, D. W., Sherman, B. T. & Lempicki, R. A. Systematic and integrative analysis of large gene lists using DAVID bioinformatics resources. *Nat. Protoc.* **4**, 44–57 (2009).
83. Wang, X., Spandidos, A., Wang, H. & Seed, B. PrimerBank: a PCR primer database for quantitative gene expression analysis, 2012 update. *Nucleic Acids Res*. **40**, D1144–D1149 (2012).
84. Li, X. et al. qPrimerDB 2.0: an updated comprehensive gene-specific qPCR primer database for 1172 organisms. *Nucleic Acids Res*. **53**, D205–D210 (2024).
85. Pertea, M., Kim, D., Pertea, G. M., Leek, J. T. & Salzberg, S. L. Transcript-level expression analysis of RNA-seq experiments with HISAT, stringTie and ballgown. *Nat. Protoc.* **11**, 1650–1667 (2016).
86. Liao, Y., Smyth, G. K. & Shi, W. featureCounts: an efficient general purpose program for assigning sequence reads to genomic features. *Bioinformatics* **30**, 923–930 (2014).
87. Love, M. I., Huber, W. & Anders, S. Moderated estimation of fold change and dispersion for RNA-seq data with DESeq2. *Genome Biol.* **15**, 550 (2014).
88. Bolger, A. M., Lohse, M. & Usadel, B. Trimmomatic: a flexible trimmer for Illumina sequence data. *Bioinformatics* **30**, 2114–2120 (2014).
89. Zhang, Y. et al. Model-based analysis of ChIP-Seq (MACS). *Genome Biol.* **9**, R137 (2008).
90. Quinlan, A. R. & Hall, I. M. BEDTools: a flexible suite of utilities for comparing genomic features. *Bioinformatics* **26**, 841–842 (2010).
91. Yu, G., Wang, L. G. & He, Q. Y. ChIPseeker: an R/bioconductor package for ChIP peak annotation, comparison and visualization. *Bioinformatics* **31**, 2382–2383 (2015).
92. Ramirez, F. et al. deepTools2: a next generation web server for deep-sequencing data analysis. *Nucleic Acids Res.* **44**, W160–W165 (2016).
93. Bailey, T. L., Johnson, J., Grant, C. E. & Noble, W. S. The MEME Suite. *Nucleic Acids Res.* **43**, W39–W49 (2015).
94. Liu, M. et al. Three-dimensional gene regulation network in glioblastoma ferroptosis. *Int. J. Mol. Sci.* **24**, 19 (2023).
95. Servant, N. et al. HiC-Pro: an optimized and flexible pipeline for Hi-C data processing. *Genome Biol.* **16**, 259 (2015).
96. Langmead, B. & Salzberg, S. L. Fast gapped-read alignment with Bowtie 2. *Nat. Methods* **9**, 357–359 (2012).
97. Robinson, J. T. et al. Juicebox.js provides a cloud-based visualization system for Hi-C data. *Cell Syst.* **6**, 256–258 (2018).
98. Li, D. et al. WashU epigenome browser update 2022. *Nucleic Acids Res.* **50**, W774–W781 (2022).

Acknowledgements

This study was funded by National Natural Science Foundation of China (81871181), Foundation of Guangzhou Municipal Science and Technology Bureau (202102010016, 2023A03J0876, 202102010163), High-tech Major Featured Technology Program of Guangzhou Municipal Health Commission (2019GX07). We thank Bullet Edits Limited for the linguistic editing and proofreading of the manuscript.

Author contributions

Conceptualization, K.J., H.L., and B.W; Methodology, K.J., B.W., X.W. and L.C.; Formal analysis, K.J., B.W., L.C. Y.J. and H.L.; Investigation, K.J., B.W., Y.C., L.W., J.B., and X.P.; Resources, G.Z., Y.J. and H.L.; Writing-Original Draft, K.J. and B.W.; Writing-Review and Editing, K.J., B.W., L.C. and H.L.; Visualization, K.J. and L.C.; Funding Acquisition, Y.J. and H.L.; Supervision, H.L.

Competing interests

The authors declare no competing interests.

Ethical approval

Primary hMSMCs were isolated from pregnant women. This study has obtained approval from the Ethics Committee of the Guangzhou Women and Children Medical Center, with the Ethics Approval Number being 201915401. All ethical regulations relevant to human research participants were followed.

Additional information

Supplementary information The online version contains supplementary material available at https://doi.org/10.1038/s42003-025-07880-9.

Correspondence and requests for materials should be addressed to Yanmin Jiang or Huishu Liu.

Peer review information *Communications Biology* thanks Tamas Zakar and the other, anonymous, reviewer(s) for their contribution to the peer review of this work. Primary Handling Editors: Kaliya Georgieva. [A peer review file is available.]